4-1-2008

# Disruption of c-Jun reduces cellular migration and invasion through inhibition of c-Src and hyperactivation of ROCK II kinase.

Xuanmao Jiao
*Kimmel Cancer Center, Thomas Jefferson University*, Xuanmao.Jiao@jefferson.edu

Sanjay Katiyar
*Kimmel Cancer Center, Thomas Jefferson University*

Manran Liu
*Kimmel Cancer Center, Thomas Jefferson University*

Susette C Mueller
*Georgetown University, Lombardi Comprehensive Cancer Center*

Michael P. Lisanti
*Thomas Jefferson University*, Michael.Lisanti@jefferson.edu



## Recommended Citation

Jiao, Xuanmao; Katiyar, Sanjay; Liu, Manran; Mueller, Susette C; Lisanti, Michael P.; Li, Anping; Pestell, Timothy G; Wu, Kongming; Ju, Xiaoming; Li, Zhiping; Wagner, Erwin F; Takeya, Tatsuo; Wang, Chenguang; and Pestell, Richard G, "Disruption of c-Jun reduces cellular migration and invasion through inhibition of c-Src and hyperactivation of ROCK II kinase." (2008). *Kimmel Cancer Center Faculty Papers.* Paper 13.
https://jdc.jefferson.edu/kimmelccfp/13

Molecular Biology of the Cell
Vol. 19, 1378–1390, April 2008

# Disruption of c-Jun Reduces Cellular Migration and Invasion through Inhibition of c-Src and Hyperactivation of ROCK II Kinase

**Xuanmao Jiao,* Sanjay Katiyar,*† Manran Liu,*† Susette C. Mueller,‡ Michael P. Lisanti,* Anping Li,* Timothy G. Pestell,* Kongming Wu,* Xiaoming Ju,* Zhiping Li,* Erwin F. Wagner,§ Tatsuo Takeya,‖ Chenguang Wang,*¶ and Richard G. Pestell*¶**

Departments of *Cancer Biology and ¶Medical Oncology, Kimmel Cancer Center, Thomas Jefferson University, Philadelphia, PA 19107; ‡Georgetown University, Lombardi Comprehensive Cancer Center, Washington, DC 20057; §Spanish Cancer Research Center (CNIO), E-28029 Madrid, Spain; and ‖Graduate School of Biological Sciences, Nara Institute of Science and Technology, Ikoma, Nara 630-0101, Japan

Submitted August 3, 2007; Revised November 28, 2007; Accepted January 10, 2008
Monitoring Editor: John Cleveland

**The spread of metastatic tumors to different organs is associated with poor prognosis. The metastatic process requires migration and cellular invasion. The protooncogene *c-jun* encodes the founding member of the activator protein-1 family and is required for cellular proliferation and DNA synthesis in response to oncogenic signals and plays an essential role in chemical carcinogenesis. The role of c-Jun in cellular invasion remains to be defined. Genetic deletion of c-Jun in transgenic mice is embryonic lethal; therefore, transgenic mice encoding a c-Jun gene flanked by LoxP sites (*c-jun*$^{f/f}$) were used. *c-jun* gene deletion reduced c-Src expression, hyperactivated ROCK II signaling, and reduced cellular polarity, migration, and invasiveness. c-Jun increased c-Src mRNA abundance and *c-Src* promoter activity involving an AP-1 site in the *c-Src* promoter. Transduction of *c-jun*$^{-/-}$ cells with either c-Jun or c-Src retroviral expression systems restored the defective cellular migration of *c-jun*$^{-/-}$ cells. As c-Src is a critical component of pathways regulating proliferation, survival, and metastasis, the induction of c-Src abundance, by c-Jun, provides a novel mechanism of cooperative signaling in cellular invasion.**

## INTRODUCTION

The protooncogene, *c-jun*, encodes the founding member of the activator protein 1 (AP-1) transcription factor family (Eferl and Wagner, 2003). Heterodimeric transcription factors of the basic region leucine zipper family, including Jun, Fos, ATF, and Maf subfamilies, bind to and regulate a broad array of target genes through conserved DNA sequences (Karin *et al.*, 1997). The *c-jun* gene encodes a protein with multiple functional domains, including an amino terminal transactivation domain, a regulatory domain, a carboxyl terminal basic DNA-binding domain and a leucine zipper protein dimerization domain. Members of the AP-1 family convey distinct functions in growth and development. c-Jun and JunB play nonredundant roles in placentation, hepatogenesis, and heart development (Eferl and Wagner, 2003).

This article was published online ahead of print in *MBC in Press* (http://www.molbiolcell.org/cgi/doi/10.1091/mbc.E07–08–0753) on January 23, 2008.

† These authors contributed equally to this work.

Address correspondence to: Richard G. Pestell (Richard.Pestell@jefferson.edu).

Abbreviations used: AP-1, activator protein 1; Cas, Crk-associated substrate; IRM, interferential reflection microscopy; JNK, c-Jun kinase; LIMK, LIM kinase; MLCK, myosin light-chain kinase; ZRP-1, zyxin-related protein 1.

Molecular analysis of the interface between AP-1 transcription factors and cell cycle control has demonstrated tightly regulated, temporally coordinated interactions between AP-1 proteins and the G1 phase cyclins, cyclins D1 and E (Pestell *et al.*, 1999; Fu *et al.*, 2004). Immunoneutralizing antibodies to c-Fos or c-Jun demonstrated a requirement for AP-1 proteins in promoting G1/S-phase transition (Riabowol *et al.*, 1988). c-*fos*$^{-/-}$, *fosB*$^{-/-}$ mice are small, and fibroblasts derived from these mice demonstrate a defect in cellular proliferation and a failure to induce cyclin D1 upon serum stimulation (Brown *et al.*, 1998). Similarly, *c-jun*$^{-/-}$ fibroblasts show a defect in cellular proliferation and a defect in apoptosis in response to genotoxic stress (Kolbus *et al.*, 2000).

In addition to cellular proliferation, c-Jun and JNK contribute to cellular migration (Xia and Karin, 2004). The JNK pathway is conserved and in *Drosophila* promotes dorsal closure through inducing epithelial cell migration. The *Drosophila* mutant *hemipterous* displays a large hole in the dorsal cuticle due to failed movement of the lateral dorsal epithelium toward the dorsal midline. The HEP protein is a homolog of the JNK-activating mitogen-activated protein kinase (DJNKK). The dorsal open phenotype is also displayed by the DJNK homolog basket (*Bsk*). Mice with a single *jnk*2 allele and no *jnk*1 alleles fail to close the neural tube and eyelids. DJNK activity is detected at the leading edge of epithelial cells and upon dorsal closure promotes ongoing expression of the transforming growth factor (TGF)-$\beta$ ho-

molog developing dorsal *decapentaplegic* (DPP; Sluss and Davis, 1997). c-Jun promotes fibroblast migration, and both c-Jun and JunB regulate migration of the mature epidermis (Eferl and Wagner, 2003; Maeda and Karin, 2003; Katiyar *et al.*, 2007). The role of c-Jun in cellular invasion and the downstream targets contributing to cellular invasiveness are poorly understood.

Cellular invasion occurs in normal developmental processes including trophoblast implantation, organogenesis, and angiogenesis. Tumor progression requires the acquisition of invasiveness through a basement membrane (Egeblad and Werb, 2002). Multiple individual cellular behaviors are required for cellular invasion, including attachment to the cellular substratum, degradation of matrix components, and migration toward diffusible chemoattractants (Balkwill, 2004). The nonreceptor tyrosine kinase c-Src contributes to cellular migration (Ishizawar and Parsons, 2004). v-Src or c-Src expression leads to disruption of intercellular adhesion and induction of in vitro invasion (Qi *et al.*, 2006). Src activity is reduced in cells in suspension, and increases, upon adhesion. Integrin ligation at the early stages of cell-matrix adhesion induces Src activity and is required for cell spreading, migration, and focal adhesion turnover (Lakkakorpi *et al.*, 2001). Src activation during the early stage of cell-matrix adhesion, corresponds to the initial deactivation of RhoA (Playford and Schaller, 2004). Conversely stable adhesive large integrin clusters are associated with suppression of Src kinase and induction of RhoA/ROCK signaling (Lin *et al.*, 2004; Janiak *et al.*, 2006). c-Src interacts with cell surface receptors (EGF family, CSF, PDGF, FGF), Shc, integrins, and FAK to promote focal adhesion turnover and promote cellular migration (Bowden and Alper, 2005).

The molecular mechanisms regulating cell motility reveal a key role for the RhoA family of small monomeric GTPases to coordinate the effects of cellular cytoskeletal adhesion. The assembly of stress fibers and their associated focal adhesions by RhoA involve downstream effectors including mouse diaphanous (mDia) and the RhoA-activated kinase ROCK. Key ROCK substrates regulating migration include the actin-depolymerizing protein cofilin, myosin light chain kinase (MLCK), and LIM kinase (LIMK; Ridley and Hall, 1992; Sahai and Marshall, 2002). ROCK activity regulates cellular migration in a cell-type–specific manner. The selective inhibitor of ROCK activity, Y27632, may either promote or inhibit cell migration depending on cellular context (Ridley and Hall, 1992; Totsukawa *et al.*, 2004). ROCK II inhibition of cells often induces a fibroblastoid morphology and increased cellular migration (Mammoto *et al.*, 2004). The increased motility of Ras-transformed cells has been attributed to a reduction in RhoA/ROCK signaling (Sahai *et al.*, 2001).

The current studies were undertaken to examine and identify the molecular mechanisms by which c-Jun regulates cellular invasiveness. Recent studies have demonstrated that cells derived from mice deleted of a target gene in ES cells may convey changes in molecular circuitry that differ from cells that are deleted of the same target gene somatically using Cre recombinase. For this reason, mice in which the *c-jun* gene was flanked by LoxP sites were used in the current studies. Excision of the *c-jun* gene by Cre recombinase demonstrated a key role for c-Jun in promoting cellular invasiveness and migratory velocity. Reintroduction of c-Jun expression rescued the defect in cellular morphology, adhesion, and migration. c-Jun inhibited ROCK and was both necessary and sufficient for the migratory phenotype. c-Jun–deficient cells demonstrated increased ROCK activity, and addition of a ROCK kinase inhibitor reversed the defect in both cellular velocity and invasiveness of *c-jun*$^{-/-}$ cells. Analysis of molecular targets for c-Jun regulating cellular migration demonstrated a reduction of c-Src abundance and an increase in ROCK II activity in *c-jun*$^{-/-}$ cells. c-Jun induced c-Src mRNA abundance and *c-Src* promoter activity, involving an AP-1 site in the *c-Src* promoter. Transduction of *c-jun*$^{-/-}$ cells with either c-Jun or c-Src expression systems reversed the defect of cellular migration in *c-jun*$^{-/-}$ cells. Collectively these studies identify a novel mechanism by which c-Jun induces c-Src expression to promote cellular migration.

## MATERIALS AND METHODS

### *Transgenic Mice, Cells, and Reagents*

Transgenic mice carrying a floxed *c-jun* allele, c-*jun*$^{f/f}$, were maintained as previously described (Eferl *et al.*, 2003). Experimental procedures with transgenic mice were approved by the ethics committee of Georgetown and Thomas Jefferson Universities. Mouse embryo fibroblasts (MEFs) were isolated from *c-jun*$^{f/f}$ mice as previously described (Albanese *et al.*, 1999). 3T3 cells were derived from *c-jun*$^{f/f}$ MEFs (Li *et al.*, 2006b) by standard protocol. Excision of the *c-jun*$^{f/f}$ allele was monitored by identification of the recombinant 600 bp per fragment as previously described (Katiyar *et al.*, 2007). A retroviral expression plasmid encoding Cre was cloned through the insertion of the cDNA from the vector pMC-Cre-PGK-Hyg (from Dr. P. Stanley, Albert Einstein College of Medicine, Bronx, NY) as an EcoRI fragment into the retroviral expression plasmid pMSCV-IRES-GFP (Neumeister *et al.*, 2003). Expression of Cre from pMSCV-IRES-GFP vector was confirmed by Western blot using an antibody directed to Cre (MMS-106). The c-Jun cDNA from pGEM c-Jun was inserted as an EcoRI fragment into the pMSCV-IRES-DsRed.

The chemical inhibitor for ROCK (Y27632) was from Calbiochem (La Jolla, CA). Rhodamine-phalloidin, AlexaFluor-488 phalloidin, and DAPI (4′,6′-diamidino-2-phenylindole) were from Sigma (St. Louis, MO). Antibodies detecting cyclin D1 (DSC-6), FAK (A-17), c-Jun (H-79), paxillin (H-114), ROCK-II (H-85), and phospho-cofilin were from Santa Cruz Biotechnology (Santa Cruz, CA). Paxillin (5H11, 05-417) and phospho-paxillin (Y31; MAB1146) mouse mAb were from Upstate Biotechnology (Charlottesville, VA). Phospho-paxillin (Y118; 44-722G) rabbit polyclonal antibody was from Biosource (Camarillo, CA). Phospho-paxillin (S178; BL854, A300-100A) was from Bethyl Laboratories (Montgomery, TX). v-Src mouse mAb (Ab-1, OP07-100UG) was from Calbiochem. AlexaFluor-488 goat anti-mouse, AlexaFluor-633 goat anti-mouse, and AlexaFluor-568 goat anti-rabbit antibodies were from Invitrogen (Carlsbad, CA). Rhodamine-X goat anti-rabbit antibody was from Jackson ImmunoResearch (West Grove, PA). Fluorescein isothiocyanate (FITC) goat anti-rabbit antibody was from Santa Cruz Biotechnology.

### *Cell Culture, Virus Production, and Reporter Gene Assays*

Retroviral vectors directed expression of green fluorescent protein (GFP) from the internal ribosomal entry site (IRES) of the MSCV vector and directed the expression of either Cre recombinase or GFP from the MSCV promoter. Recombinant retrovirus was produced as previously described (Li *et al.*, 2006b). MSCV retroviruses were prepared by transient cotransfection with helper virus into 293T cells, using calcium phosphate precipitation. The retroviral supernatants were harvested 48 h after transfection and filtered through a 0.45-$\mu$m filter. *c-jun*$^{f/f}$ 3T3 cells were incubated with fresh retroviral supernatants in the presence of 8 $\mu$g/ml polybrene for 24 h, cultured for a further 4 d, and subjected to fluorescence-activated cell sorting (FACS; FACStar Plus; BD Biosciences, San Jose, CA) to select for cells expressing GFP. *c-jun*$^{f/f}$ 3T3 cells expressing either MSCV-IREF-GFP or MSCV-Cre-IRES-GFP were subsequently subcloned. Analyses were conducted with at least three separate colonies of each line. Cells were maintained in DMEM supplemented with 5% FBS, 100 $\mu$g/ml penicillin and streptomycin and were cultured in 5% $CO_2$ at 37°C. For c-Jun rescue experiments, *c-jun*$^{-/-}$ 3T3 cells were infected with ether MSCV-c-Jun-DsRed or its control vector as described above. The cells with red fluorescence were sorted by FACS and subsequently used for analysis. Fluorescence phase-contrast imaging was carried out using the 10× objectives of an Olympus IX microscope (Melville, NY).

Luciferase reporter gene assays were conducted using the 1.9-kb murine c-Src wild-type (wt) and AP-1 point mutant luciferase reporter genes (Kumagai *et al.*, 2004). Luciferase activity was determined upon normalization of transfection efficiency using a cotransfected $\beta$-galactosidase reporter gene (Katiyar *et al.*, 2007).

Primary mammary epithelial cell (MEC) culture was based on the reference (Wulf *et al.*, 2004) with modification. Mammary glands from 8- to 12-wk-old virgin mice were dissociated by chopping and then digested with 0.4 mg/ml collagenase in MEC culture media (Ham's F12 with 10% FBS, 1× MEM nonessential amino acids, 100 $\mu$g/ml penicillin and streptomycin, 50 $\mu$g/ml gentamicin, 4 $\mu$g/ml insulin, 1 $\mu$g/ml hydrocortisone, 10 ng/ml EGF, 10 ng/ml cholera toxin) in 5% $CO_2$ at 37°C for 18 h. The digested material was

homogenized by pipetting up and down and then was washed with PBS with 50 $\mu$g/ml gentamicin three times. The pellet was resuspended in MEC culture in a 10-cm plate and then cultured for 4 h to remove fibroblasts. The suspension was divided into several plates according to the requirement of the experiments. After 3–5 d culture, the MECs were treated with ether control adenovirus or adeno-Cre1 ($2 \times 10^8$ PFU/ml) for 24 h, washed with fresh MEC culture media, and then continually cultured for another 4 d.

### *Phalloidin Staining and Quantification and Cell Diameter Assessment*

Phalloidin staining was conducted as previously described (Neumeister *et al.*, 2003). The image of phalloidin staining and quantification was conducted using ether confocal microscopy or FACS analysis. Clones of primary transduced 3T3 cells were harvested and washed in PBS. The cell pellets were fixed with 4% paraformaldehyde and permeabilized with 0.05% NP-40. Subsequent to PBS washing, cells were stained with rhodamine-phalloidin and DAPI. Cell diameter was assessed using a Multisizer 3 instrument (Beckman Coulter, Miami, FL).

### *Western Blotting and RT-PCR*

Whole cell lysates (60 $\mu$g) were separated by 10% SDS (SDS-PAGE), and the proteins were transferred to nitrocellulose membranes for Western blotting as previously described (Li *et al.*, 2006b). Western blotting was used to assess protein stability in the presence of cycloheximide as previously described (Li *et al.*, 2006a). mRNA abundance was determined by RT-PCR using primers directed to murine c-Src mRNA ordered from Qiagen (Chatsworth, CA; QT00103691, Mm_Src_1_SG QuantiTect Primer Assay). The primer directed to 18S mRNA from Qiagen (QT01036875, Mm_Rn18s_2_SG QuantiTect Primer Assay) was used as control.

### *Cellular Migration Assays*

Cells were seeded in a 12-well plate 24 h before being placed in an incubator on the microscope to maintain the temperature at 37°C and $CO_2$ at 5%. The cell movement videos were taken at 5-min intervals using a Nikon Eclipse TE-300 inverted microscope system (Melville, NY). The cell movement velocity was determined by tracing the single cells at different time points using

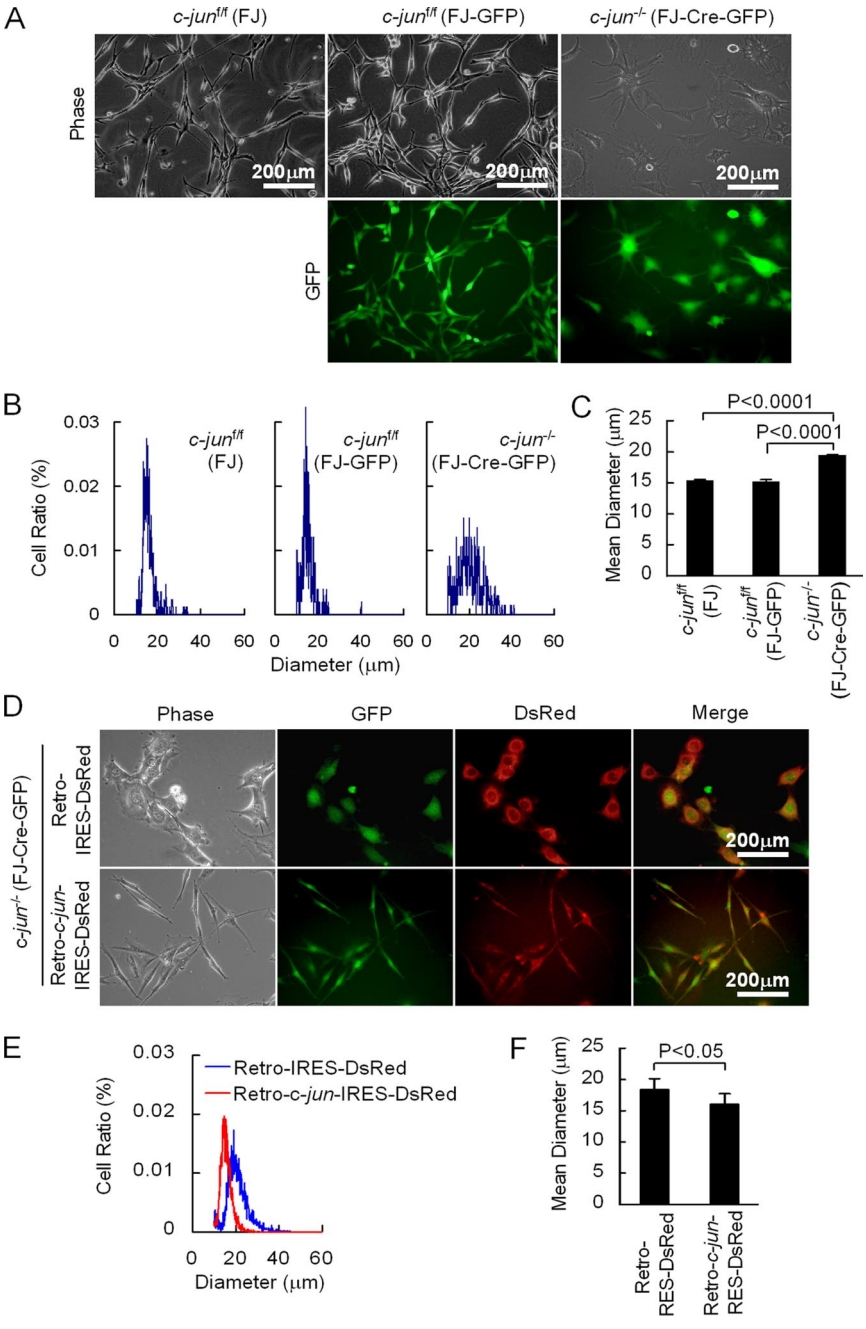


**Figure 1.** c-Jun reduces cellular diameter. (A) *c-jun*$^{f/f}$ 3T3 cells were transduced either with retrovirus encoding GFP or Cre-GFP. Cellular diameter was determined by FACS and the cellular diameter is shown. (B and C) *c-jun*$^{f/f}$ 3T3 cells transduced with Cre and deficient in c-Jun were transduced with either retrovirus encoding DsRed protein or c-Jun-DsRed. Phase-contrast and fluorescent microcopy was conducted. (D and E) Cellular diameter of *c-jun*$^{f/f}$ 3T3 cells transduced with either the retro-IRES-DsRed or c-Jun IRES-DsRed. (F) The mean cellular diameter is shown in $\mu$M.

MetaMorph software (Molecular Devices, Downingtown, PA). To observe the effect of ROCK or c-Src inhibition, cells were treated with 10 $\mu$M Y27632 or 2 $\mu$M SU6656 (Calbiochem) for 30 min before and during the course of time-lapse recording. Transwell migration assays were conducted using a transwell chamber, and cells were counted after 3 h of treatment for cell migration (Li *et al.*, 2006b).

The migration of MECs was assessed by wound healing assay. Cells were grown to confluence on six-well plates, and the monolayers were wounded with a P10 micropipette tip. MEC culture media was changed immediately after wounding. The wound-healing videos were taken at 20-min intervals for 24 h using a Nikon Eclipse TE-300 inverted microscope system (Melville, NY). The cell movement velocity was also determined by MetaMorph.

### *Immunofluorescence*

*c-jun*$^{f/f}$ and *c-jun*$^{-/-}$ 3T3 cells grown in four-well chambers, and slides were fixed with 4% paraformaldehyde in PBS for 20 min at room temperature. The slides were rinsed with PBS and permeated with 0.05% NP-40 in PBS. The primary antibodies used were mouse monoclonal anti-paxillin (clone 5H11; Upstate Biotechnology; 1/100) and rabbit polyclonal anti-phospho-paxillin (pY118; Biosource; 1/100). The secondary antibodies used were Alexa Fluor 633–conjugated F(ab')$_2$ fragment of goat anti-mouse immunoglobulin G (IgG; Molecular Probes, Eugene, OR; 1/250) and rhodamine red X–conjugated goat anti-rabbit IgG (Jackson ImmunoResearch Laboratories; 1/50). Fluorescence confocal imaging was acquired with either a 60× objective of an Olympus IX70 laser confocal microscope (Georgetown University) or a 63× objective of a Zeiss LSM510/META laser confocal microscope (Thomas Jefferson University). The images were processed with MetaMorph (Molecular Devices).

### *Interferential Reflection Microscopy*

Interferential reflection microscopy (IRM) images were collected using an Olympus Fluoview FV300 laser scanning microscope outfitted with a 60×/1.4 NA oil immersion lens. Cells were cultured on dishes with number 1.5 coverslips affixed to the bottom and then transferred to a heated stage (37°C) in complete medium with 10 mM HEPES, pH 7.4, added to maintain constant pH (Li *et al.*, 2006b). The samples were illuminated with 488-nm argon laser light, and reflected light images were collected from channel 2 in the absence of emission filters. During live imaging, rapid and local changes in interference patterns or "flickering" occur. To better visualize longer-lived focal adhesion formation and changes that take place in their number and shape over time (minutes), images were averaged over time (seconds) to eliminate short-lived fluctuations. Focal adhesions appear as dark streaks, whereas close contacts or membrane distances that are greater appear lighter. At even greater distances, evidence of cell contact is not apparent. Each focal adhesion was tracked using MetaMorph and the life of focal adhesion was calculated based on the frames of focal adhesion existence.

### *Fluorescent-Gelatin Degradation Assay*

AlexaFluor-568–conjugated gelatin matrix degradation experiments were carried out on triplicate coverslips with analysis of at least 25 fields per coverslip (100 cells minimum and at least three iterations of each experiment). Dark spots on the bright, fluorescent gelatin matrix were thresholded. For each field (0.01 mm$^2$), the area of the degraded zones ($\mu$m$^2$) and the area of cells ($\mu$m$^2$; determined by FITC-phalloidin staining) were summed, and the total area of degraded zones per cell area was calculated for each field of view. Matrix degradation is reported as area degraded per cell area.

### *ROCK Activity Assay*

Rho-associated protein kinase (ROCK) activity was assessed by the Rho-kinase Assay Kit from Cclex Co. (Nagano, Japan) according to the manufacturer's protocol. The phospho-specific mAb used in this kit recognizes the phospho-threonine 697 residue in MBS/MYPT1, which is phosphorylated by ROCK. For each sample, 10 $\mu$l of 1 mg/ml cell lysate was used. The absorbance value obtained from ROCK inhibitor (Y27632)-treated lysates was subtracted from total absorbance to exclude the influence of other kinases.

### *c-Src Kinase Activity Assay*

c-Src kinase activity was assessed by combination of immunoprecipitation (IP) activity Src Kit (Calbiochem) and HTScan Src Kinase Assay Kit (Cell Signaling, Beverly, MA). c-Src from cell lysate (400 $\mu$g protein) was immunoprecipitated by IP activity Src Kit according to the manufacturer's manual. The kinase activity of immunoprecipitated c-Src was measured with HTScan Src Kinase Kit based on the manufacturer's manual.

### *Statistical Analysis*

Statistical significance was determined by Student's *t* test.

## RESULTS

### *c-Jun Deletion Induces Cellular Spreading and F-Actin*

To examine the role of c-Jun in cellular migration, fibroblasts were derived from mice carrying a floxed *c-jun* allele (Supplement 1A). *c-jun*$^{f/f}$ 3T3 cells were derived and transduced with retroviral expression plasmids encoding either GFP or Cre recombinase. GFP-expressing clones were selected for subsequent analysis. The excision of the *c-jun* allele resulted in the formation of a 600-base pair PCR product (Supplement 1A). Deletion of the *c-jun* allele resulted in a complete loss of c-Jun by Western blot analysis (see Figure 3C) or by FACS analysis (Supplement 1B) and immunostaining (Supplement 1D). Cells deleted of *c-jun* exhibited a flattened morphology in culture compared with the polarized fibroblastoid morphology of *c-jun*$^{f/f}$ 3T3 cells transduced with a GFP expression vector (Figure 1A).

In view of the apparent increase in cellular diameter of the *c-jun*$^{-/-}$ cells, cellular circumference was assessed in cellular suspension using a Multisizer 3 (Beckman Coulter). Cellular diameter was increased 22% ($p < 0.05$; Figure 1, B and C). To determine whether the change in cellular morphology was due to c-Jun rather than a secondary event, the *c-jun*$^{-/-}$ cells were transduced with a retrovirus expressing c-Jun. Reintroduction of c-Jun expression into *c-jun*$^{-/-}$ cells was sufficient for the rescue of the fibroblastoid-polarized morphology and cellular diameters by FACS analysis (Figure 1, D–F).

A flattened nonpolarized morphology frequently correlates with reduced cellular migration. To determine whether c-Jun regulated cellular migration, transwell migration assays were conducted using a Boyden chamber. Comparison was made between *c-jun*$^{f/f}$ 3T3 cells, cells deleted of *c-jun* using retroviral Cre, and cells retransduced with a retroviral vector encoding c-Jun tagged through an internal ribosomal entry site to red fluorescent protein (DsRed). The deletion of c-Jun reduced cellular transmigration by 60% (Figure 2A). Reintroduction of c-Jun into *c-jun*$^{-/-}$ cells restored the migratory phenotype (Figure 2A) and restored c-Jun abundance, as assessed by Western blot analysis (Figure 2B).

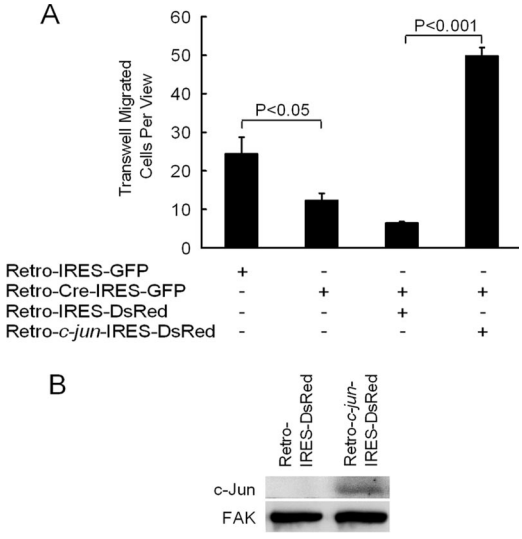


**Figure 2.** c-Jun induces cellular migration. (A) Transwell migration assays were conducted using *c-jun*$^{f/f}$ 3T3 cells transduced with either GFP, Cre-GFP, DsRed, or c-Jun-DsRed. The data are shown as the mean number of cells migrated. (B) Western blot analysis for c-Jun demonstrating transduction of *c-jun*$^{-/-}$ cells with the c-Jun expressing retrovirus.

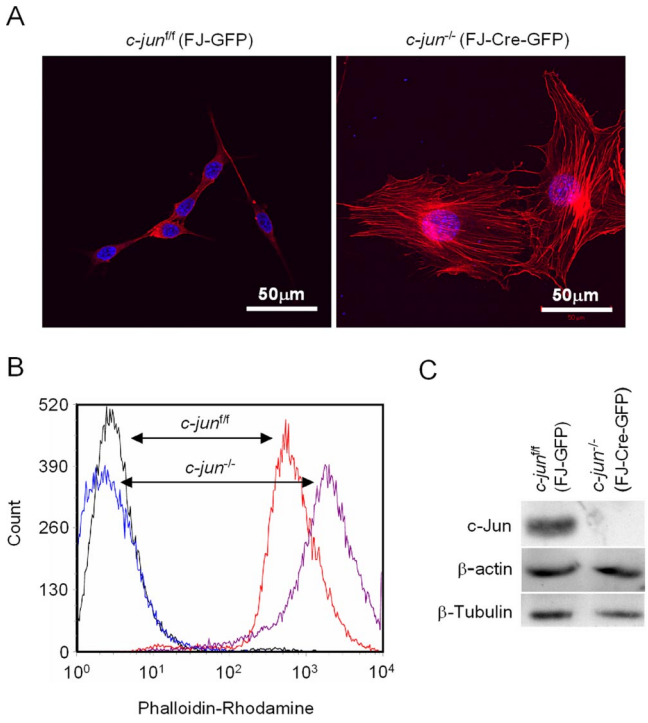


**Figure 3.** c-Jun induction of F-actin. (A) F-actin staining with phalloidin and nuclear staining with DAPI, demonstrates the fibroblastoid morphology of *c-jun*$^{f/f}$ (wt) cells, and the epitheliod morphology of *c-jun*$^{-/-}$ cells. (B) Quantitation of F-actin staining by FACS analysis demonstrates a 2.5-fold increase in F-actin in *c-jun*$^{-/-}$ cells. (C) Western blot analysis shows deletion of c-Jun protein, compared with control proteins $\beta$-tubulin and $\beta$-actin.

To assess whether c-Jun regulated altered cellular morphology and migration through changes in actin stress fiber formation, phalloidin staining was conducted (Figure 3). 3T3 wt cells demonstrated peripheral F-actin staining (Figure 3A). In c-Jun–deficient cells, F-actin staining was disorganized with a perinuclear distribution, with increased F-actin throughout the cytoplasm (Figure 3A). Quantitation of F-actin by FACS demonstrated an increase in total F-actin in *c-jun*$^{-/-}$ cells compared with *c-jun*$^{f/f}$ (Figure 3B). Western blot analysis of the cells demonstrated a reduction in the abundance of c-Jun, normalized to the control proteins, $\beta$-actin or $\beta$-tubulin (Figure 3C).

### *c-Jun Governs Paxillin Tyrosine 31, 118, and serine 178 Phosphorylation within Focal Contacts*

To determine whether the increase in F-actin was associated with increased focal contacts, immunohistochemistry was conducted of focal contacts. The coronal view of the *c-jun* wt and *c-jun*$^{-/-}$ 3T3 cells demonstrated the flattened and spread morphology of the *c-jun*$^{-/-}$ cells (Figure 4A). The distribution of paxillin, marking focal contacts, evidenced the centripetal distribution of focal contacts at the periphery of the *c-jun*$^{-/-}$ cells. Focal contacts were identified at the distal aspect of the F-actin cables in the higher magnification images (Figure 4B). Analysis of focal contacts was conducted using FAK and phosphorylated paxillin as markers for focal contacts (Figure 5). Consistent with previous studies, 3T3 cells showed a diffuse distribution of cytoplasmic paxillin, with relatively few focal contacts at the polar ends of the cell as determined by FAK (Figure 5A) and by costaining of paxillin with tyrosine-phosphorylated paxillin (Figure 5B). In contrast, the *c-jun*$^{-/-}$ cells demonstrated increased focal contacts with FAK (Figure 5A) and tyrosine-phosphorylated

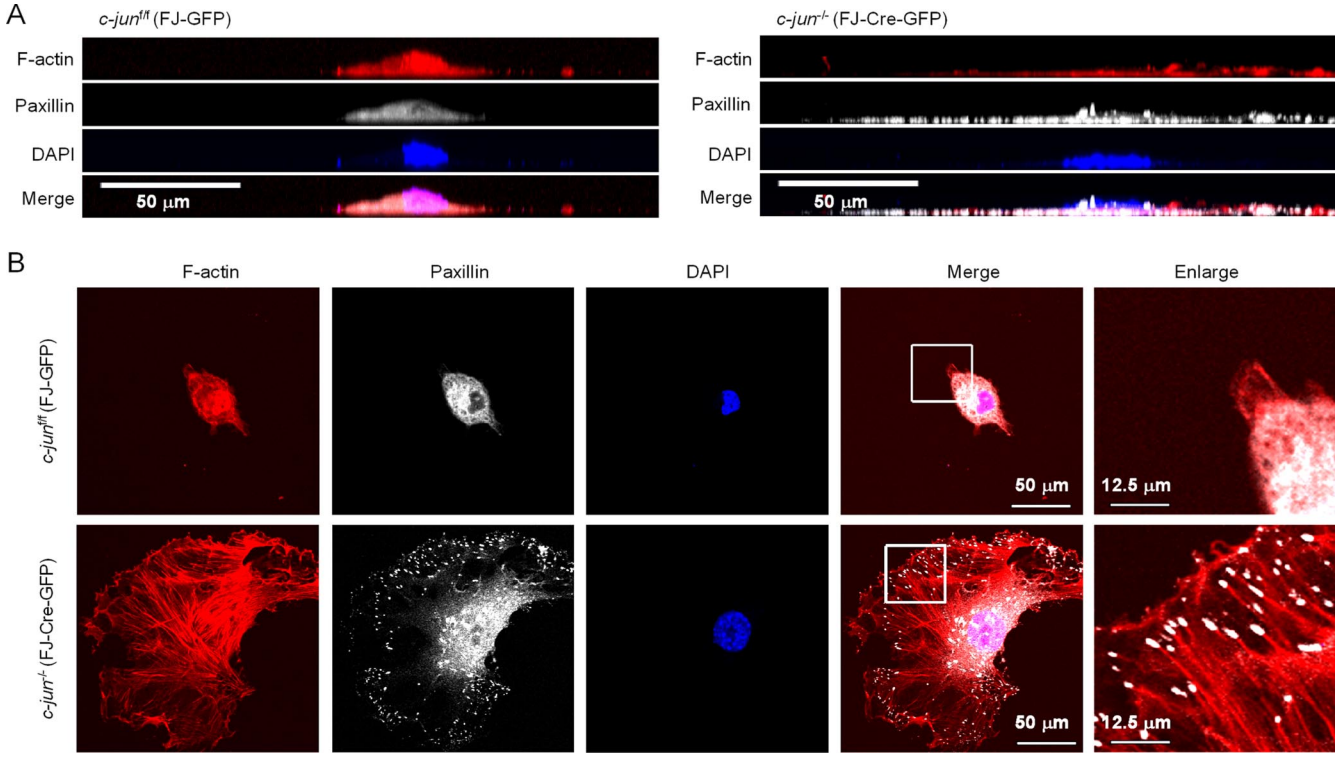


**Figure 4.** c-jun excision induces formation of paxillin at F-actin tips. (A) coronal section of cells stained for F-actin and paxillin demonstrates flattened spread morphology of *c-jun*$^{-/-}$ cells with paxillin marking focal contacts throughout the cell base, (B) seen distributed centripetally around the cells circumference.

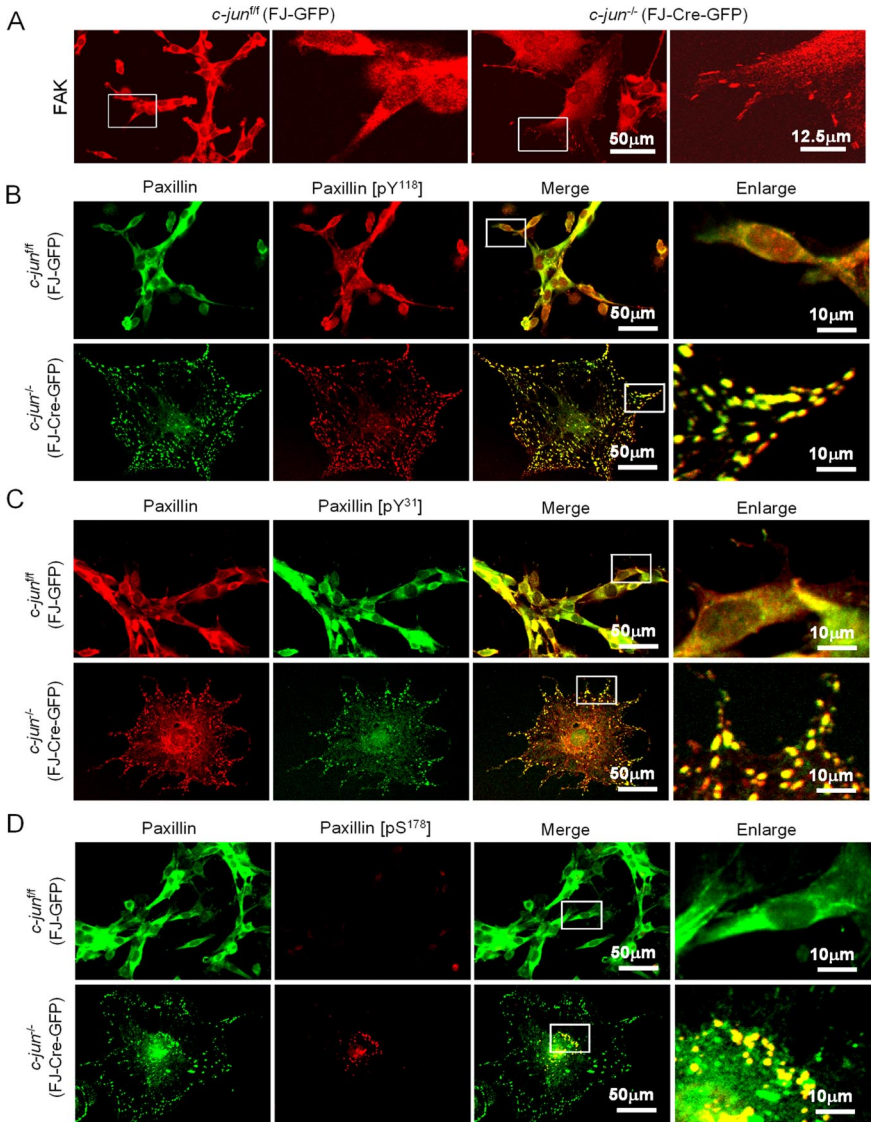


**Figure 5.** c-jun excision induces large focal contacts in a centripetal distribution. (A) *c-jun*$^{f/f}$ 3T3 cells were transduced either with control vector GFP or Cre expression vector (pMSCV-Cre-IRES-GFP). Immunostaining was conducted for FAK (A) and for (B–D) paxillin and phosphopaxillin Y118 (B), Y31 (C), and S178 (D). The merged image of paxillin and phosphopaxillin are enlarged in the fourth image of each series. Note the formation of large focal contacts at the cell periphery, and in D note the perinuclear distribution of phosphorylated paxillin (Serine 118).

paxillin, forming multiple small, peripherally organized focal contacts, distributed circumferentially around the cell (Figure 5B). Association between c-Src and FAK results in c-Src activation and the sequential association with paxillin (Brown and Turner, 2004; Schlaepfer *et al.*, 2004). In addition to permitting recruitment of multiple binding proteins to focal contacts, paxillin is phosphorylated at specific tyrosine and serine residues in response to growth factors and cytokines and upon association of c-Src. Confocal microscopy was undertaken using phospho-specific antibodies directed to specific paxillin phosphorylation sites to investigate altered extracellular signaling pathways of *c-jun*$^{-/-}$ cells (Brown and Turner, 2004). Activated c-Src and FAK induces tyrosine phosphorylation at tyrosine residue 118 and residue 31. Multiple centripetally distributed tyrosine 118 phosphorylated foci were observed in *c-jun*$^{-/-}$ cells (Figure 5B). Adhesion induced phosphorylation by FAK, induces paxillin tyrosine phosphorylation at amino acid residue 31. Wild-type 3T3 cells exhibited little activation of paxillin at Y31. However, increased phosphorylation was observed in focal contacts of the *c-jun*$^{-/-}$ cells (Figure 5C). Serine 178 of paxillin serves as a substrate for JNK phosphorylation. Increased phosphorylation of paxillin at serine 178 was observed in a perinuclear distribution of *c-jun*$^{-/-}$ cells (Figure 5D). Thus, *c-jun*$^{-/-}$ cells demonstrate hyperactivation of paxillin phosphorylation, and the phosphorylated paxillin is located circumferentially associated with increased F-actin stress fiber formation.

The focal adhesions of *c-jun*$^{-/-}$ cells are large. Large focal adhesions normally do not undergo rapid turnover, tending to be involved passively in anchorage, whereas fast-moving cells usually do not form focal adhesions (Beningo *et al.*, 2001). In view of the increased spreading and reduced migration of *c-jun*$^{-/-}$ cells, we assessed focal adhesion stability by examining the relative contact of the cell to its substratum using IRM with time-lapse videomicroscopy. IRM measures the appositional proximity of cells with their substratum. The areas of contact between the cell and its substratum, such as focal adhesions, are displayed as dark structures. Less closely opposed areas of the cell exhibit gradients of gray to white (Neumeister *et al.*, 2003). The number and surface area of contact points between the cell and its substratum was dramatically enhanced in *c-jun*$^{-/-}$ cells at 0 min (Figure 6A). Serial images of the cells were obtained by IRM

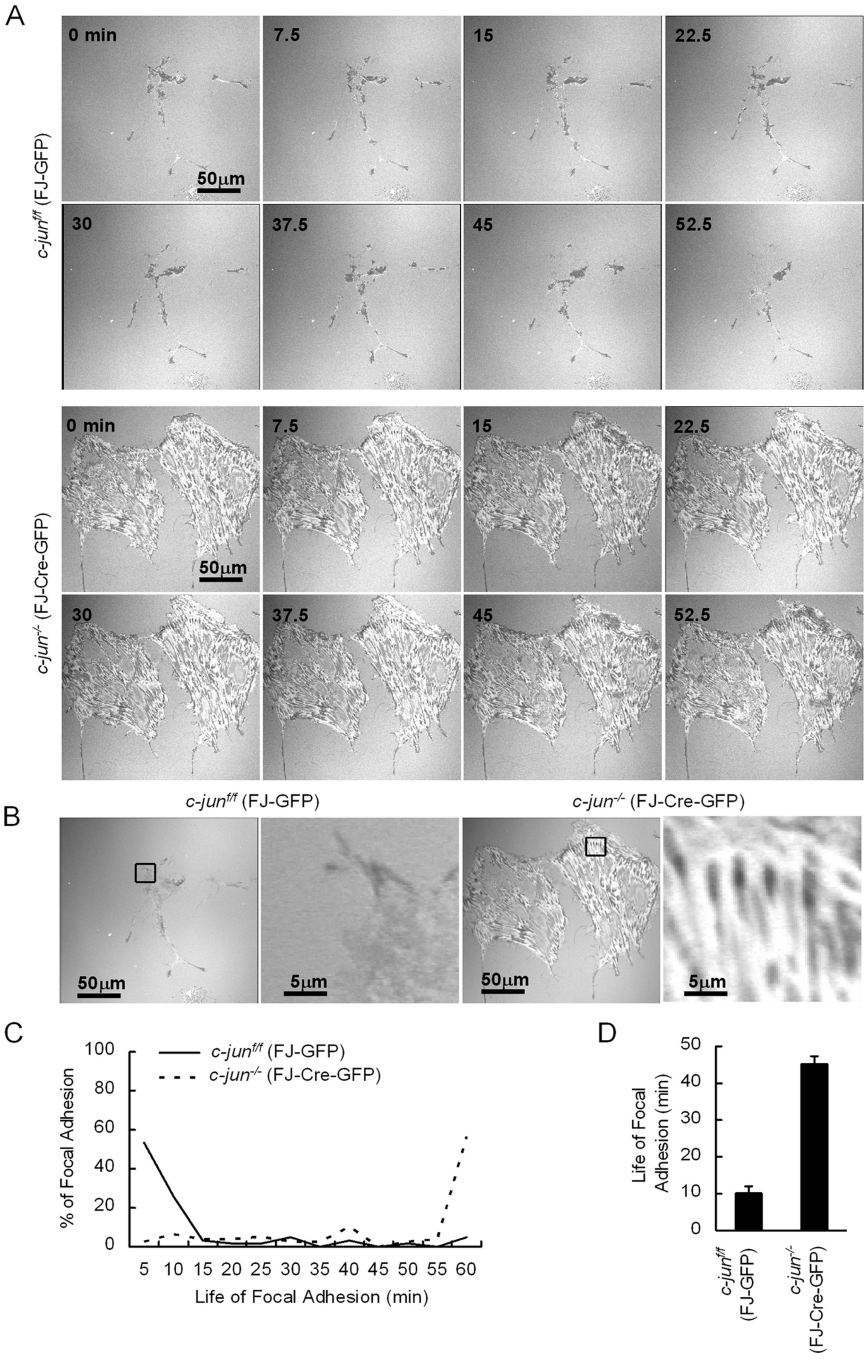


**Figure 6.** c-Jun regulates cellular adhesion stability. (A) Interferential refraction microscopy conducted with time-lapse microscopy was used to monitor the stability of focal contacts. Deletion of c-Jun induces large stable focal contacts seen at high magnification in B. (C) Quantitation of the life of focal adhesions from videomicroscopy with (D) Mean data ± SEM for the life of focal adhesions as described in *Materials and Methods.*

to determine the stability of the focal adhesion (Li *et al.*, 2006b). Focal adhesion dynamics were analyzed by videomicroscopy to determine the stability of focal adhesions. Focal contacts turned over rapidly in 3T3 wt control cells. In contrast focal adhesions turned over poorly in *c-jun*$^{-/-}$ cells, with prominent static wedge-like IRM density observed in *c-jun*$^{-/-}$ cells (Figure 6B). The rate of turnover of focal adhesions correlates with cellular motility. Focal contacts that are remodeled rapidly are associated with enhanced rates of cellular migration. To determine whether c-Jun regulates the rate of focal contact turnover quantitative videomicroscopy studies were conducted as previously described (Smilenov *et al.*, 1999; Ren *et al.*, 2000). The mean life of focal contacts in *c-jun*$^{f/f}$ cells was ~10 min, whereas the focal contact of *c-jun*$^{-/-}$ cells was ~45 min (Figure 6, C and D). Thus, the rate of turnover of focal adhesions correlated with cellular motility (Figure 2). Focal adhesions that were remodeled rapidly were associated with enhanced rates of cellular migration, whereas the loss of c-Jun increased their lifetime and slowed migration.

### *c-Jun Inhibits ROCK II*

Increased F-actin formation, as seen in *c-jun*$^{-/-}$ cells, is observed with increased ROCK II and Rho activity (Amano *et al.*, 1997). ROCK is known to activate JNK. As JNK phosphorylates paxillin at serine 178, the increased phosphorylation of paxillin S178 in *c-jun*$^{-/-}$ cells also raised the possibility that ROCK activity was increased in *c-jun*$^{-/-}$ cells.

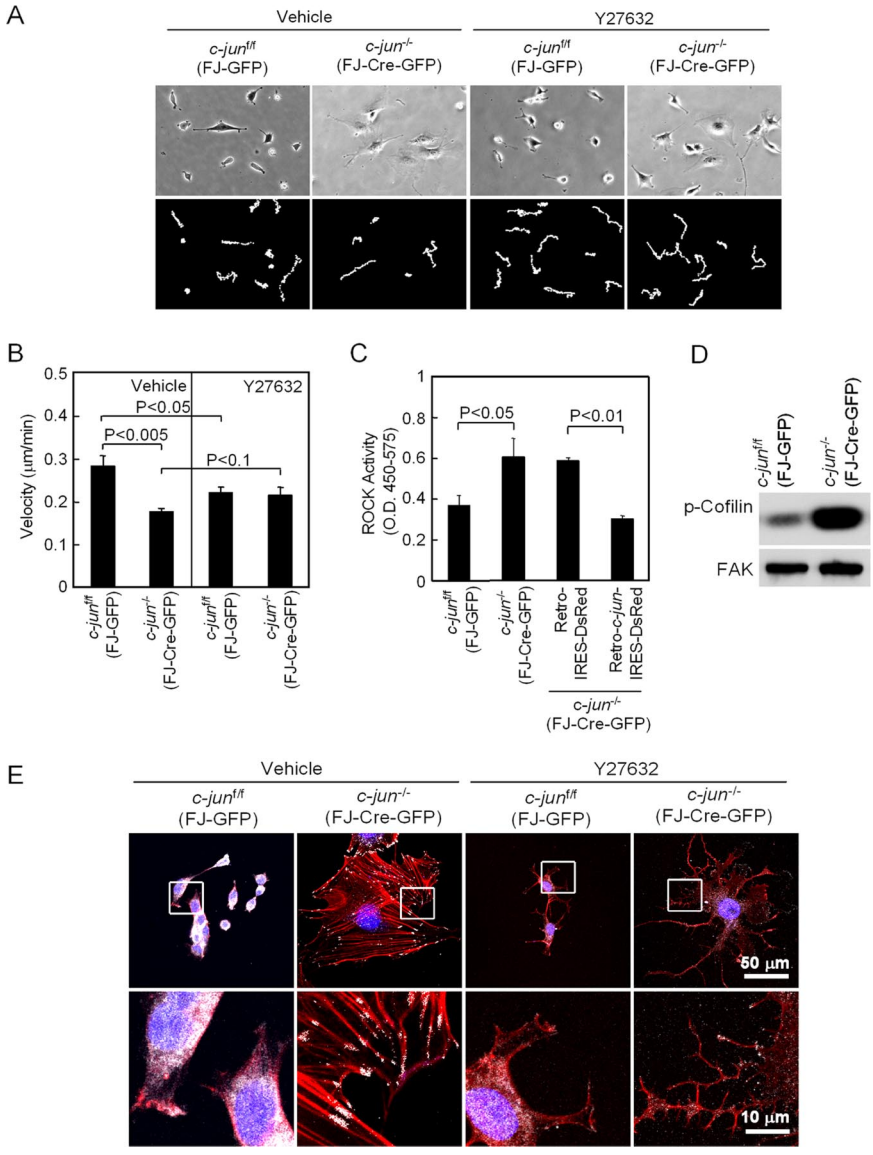


**Figure 7.** c-Jun induction of cellular velocity involves ROCK kinase. (A) The cellular velocity was determined by videomicroscopy. (B) *c-jun*$^{-/-}$ cells show reduced velocity ($p < 0.005$) compared with *c-jun*$^{f/f}$ cells, which is restored ~25% by treatment with the ROCK kinase inhibitor (Y27632, 10 $\mu$M). (C) The ROCK activity is increased upon deletion of c-Jun ($p < 0.05$). Reintroduction of c-Jun inhibits ROCK activity to that of *c-jun*$^{f/f}$ cells (D). Western blot analysis of phosphorylated cofilin, a marker of ROCK activation with FAK used as a loading control. (E) Phalloidin staining of cells at (600×) and (3000×) treated with vehicle or 10 $\mu$M Y27632.

Our studies of transwell cell migration demonstrated reduced migration in *c-jun*$^{-/-}$ cells and the induction of migration by c-Jun reintroduction. Cellular migration involves several components including migratory velocity and persistence of migratory directionality. To examine further the mechanisms by which c-Jun regulated migration, time-lapse videomicroscopy was used to characterize the defect in migration of *c-jun*$^{-/-}$ cells. *c-jun*$^{-/-}$ cells showed a 40% decrease in cellular migration velocity ($p < 0.05$; Figure 7, A and B). Addition of the ROCK II kinase inhibitor Y27632 eliminated the difference in migration velocity between the c-Jun–expressing and *c-jun*$^{-/-}$ cells, suggesting hyperactive ROCK II kinase contributed to the defect in cellular migratory velocity. ROCK II kinase inhibition of 3T3 cells increased migratory velocity consistent with the known role of ROCK II in basal migratory velocity of 3T3 cells (Figure 7B). To confirm that ROCK II kinase activity is increased after loss of *c-jun* and that it is restored after reintroduction of *c-jun*, the effect of c-Jun on ROCK II kinase activity was assessed in *c-jun*$^{-/-}$ cells using the myosin-binding subunit of myosin phosphatase as substrate. ROCK II kinase activity was increased in *c-jun*$^{-/-}$ cells (Figure 7C). Reintroduction of c-Jun to physiological levels restored ROCK II activity (Figure 7C). As an additional assay of ROCK II activity the phosphorylation of the ROCK II substrate cofilin was determined. The actin-depolymerizing protein cofilin is phosphorylated by ROCK and LIM kinase, inhibiting its actin-depolymerizing activity, thereby stabilizing actin stress fibers. Consistent with the increase in ROCK II kinase activity, phosphorylation of cofilin was increased in *c-jun*$^{-/-}$ cells (Figure 7D). To determine whether the increased stress fiber formation in *c-jun*$^{-/-}$ cells was in part dependent on ROCK hyperactivation, phalloidin staining was conducted (Figure 7E). *c-Jun*$^{-/-}$ cells demonstrated increased stress fiber formation. Costaining with paxillin identified focal adhesions at the centripetal end of F-actin cables, seen more clearly with fivefold magnification (bottom panels, Figure 7E). Addition of the ROCK inhibitor Y27632 had little effect on distribution of phalloidin in wt cells, but reduced the appearance of stress fibers and paxillin-containing focal adhesions in *c-jun*$^{-/-}$ (Figure 7E). These findings are consistent with a role for hyperactivated ROCK in the increased stress fiber formation of *c-jun*$^{-/-}$ cells.

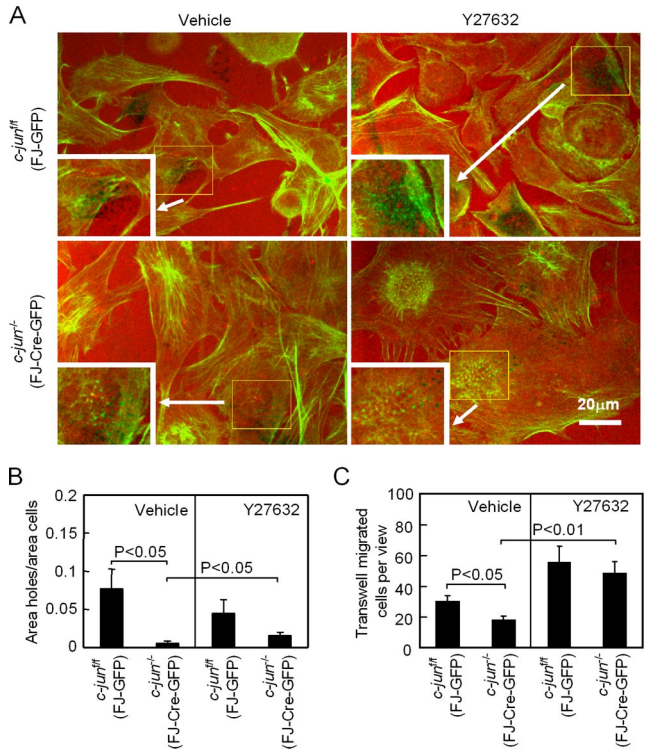


**Figure 8.** c-Jun induction of invasion involves ROCK kinase. (A) Invadopodia assays were conducted of *c-jun*$^{f/f}$ 3T3 cells in the presence of either GFP or Cre plus GFP. Holes indicating active invadopodia are shown in black. Cells were treated either with control or the ROCK kinase inhibitor Y27632 for 12 h. The top series of panels are shown with magnification in the inset of each panel at bottom left of the region enclosed within the white frame. (B) The *c-jun*$^{f/f}$ or *c-jun*$^{-/-}$ cells were assessed for the number of holes. Data are mean ± SEM of n > 20 separate frames. c-Jun deletion reduces invadopodia ($p < 0.05$). Treatment with Y27632 increases the invasion of *c-jun*$^{-/-}$ cells threefold ($p < 0.05$). (C) Transwell invasion assays conducted in a Boyden chamber showed similar results as in B.

### *c-Jun Induces Cellular Invadopodia and c-Src Expression*

Invasive cells extend lamellipodial protrusions and invade extracellular matrix. The abundance of matrix degradation associated with this protrusive activity correlates with invasive potential. Invadopodia can be assessed through extracellular matrix degradation (Bowden *et al.*, 2001). The ability of 3T3 cells to proteolyze gelatin matrix was assessed using an AlexFluor 568 coupled to ECM substrate (gelatin; AlexFluor 568). The presence of invadopodia, evidenced by matrix degradation, results in dark areas and fluorescence (Figure 8A). The deletion of *c-jun* abrogated by 80% the amount of ECM substrate degraded by invadopodia (Figure 8B).

The role of ROCK II in invadopodia formation was next assessed (Figure 8A). The breast cancer cell line MDA-MB-231 transformed with v-Src increased invadopodia activity (data not shown). 3T3 cells treated with the ROCK inhibitor reduced invasiveness, but this reduction was not statistically significant. Consistent with a model in which c-Jun inhibition of ROCK kinase promoted invadopodia, *c-jun*$^{-/-}$ cells treated with ROCK inhibitor increased invadopodia formation threefold (Figure 8B). To determine the role of *c-jun* and *c-jun*–mediated repression of ROCK II kinase in migration across a membrane, transwell migration assays were conducted in a Boyden chamber (Figure 8C). The ROCK II inhibitor did not fully restore cell invasiveness, indicating ROCK II–independent pathways are also involved. Together, these studies demonstrate the abundance of c-Jun regulates ROCK II activity. Increased ROCK II activity in *c-jun*$^{-/-}$ cells contributes to both reduced cellular migration and reduced cellular invasion.

### *c-Jun Induction of Migration Is Dependent on ROCK and Src Kinase*

To examine further the mechanism by which c-Jun may inhibit ROCK activity, we considered upstream regulators of ROCK activity as potential targets of c-Jun. c-Src inhibits ROCK II activity (Pawlak and Helfman, 2002). We therefore examined the relative abundance of c-Src, in *c-jun*$^{-/-}$ and wt 3T3 cells. c-Src abundance as well as src kinase activity was reduced in *c-jun*$^{-/-}$ cells (Figure 9, A and G). Reintroduction of c-Jun into *c-jun*$^{-/-}$ cells restored c-Src abundance, indicating that c-Src is induced by c-Jun (Figure 9A, lanes 3 vs. 4).

To determine the mechanisms by which c-Jun induced c-Src abundance, the mRNA levels of c-src were determined by RT-PCR in *c-jun*$^{f/f}$ versus *c-jun*$^{-/-}$ cells (Figure 9B). Compared with 18S mRNA, c-src mRNA were 2.5-fold greater in *c-jun*$^{f/f}$ than in *c-jun*$^{-/-}$ cells. To determine whether c-jun was capable of enhancing the activity of the *c-src* promoter, a 1.9-kb c-Src promoter luciferase reporter was assessed (Figure 9C). Comparison of relative promoter activity was conducted in *c-jun*$^{f/f}$ versus *c-jun*$^{-/-}$ cells, with normalization of transfection efficiency conducted using a β-galactosidase, control reporter gene. The activity of the *c-src* promoter was reduced ~80% upon deletion of the *c-jun* gene (Figure 9C). To determine the role of the *c-src* promoter putative AP-1 site, comparison was made between wt *c-src* promoter and the activity of a *c-src* promoter construction encoding a point mutation within the *c-src* promoter AP-1 site. Mutation of the AP-1 site reduced *c-src* promoter activity ~90% (Figure 9C). Together these studies demonstrate endogenous c-jun abundance regulates activity of the *c-src* promoter through its AP-1 site.

Consistent with a model in which increased c-Src activity contributes to increased migratory velocity mediated by endogenous c-Jun, addition of the Src kinase inhibitor SU6656 reduced migratory velocity of wt cells to that of *c-jun*$^{-/-}$ cells (Figure 9, D and E). To determine whether the reduction in c-Src abundance in *c-jun*$^{-/-}$ cells was responsible for the hyperactive ROCK activity, ROCK kinase assays were conducted (Figure 9F). Addition of SU6656 inhibited src kinase activity (Figure 9G) and enhanced ROCK activity >2.5-fold (Figure 9F), consistent with a model in which c-Src inhibits ROCK kinase activity. The reduction of c-Src abundance in *c-jun*$^{-/-}$ cells correlated with increased ROCK activity. The presence of hyperactive ROCK in *c-jun*$^{-/-}$ cells was characterized by increased stress fiber formation with paxillin at the terminal ends of F-actin bundles (Figure 4B). To determine the role of hyperactive c-Src activity in this phenotype, paxillin and F-actin staining was conducted of either wt or *c-jun*$^{-/-}$ cells treated with Src inhibitor. F-actin staining demonstrated that the addition of Src kinase inhibitor to wt cells induced F-actin stress fiber staining associated with formation of focal paxillin staining at the F-actin ends resembling *c-jun*$^{-/-}$ cells (Figure 9H).

These studies demonstrated that c-jun deletion reduced c-Src abundance and cellular motility. To determine whether restoration of c-Src abundance could restore cellular motility, a retroviral expression vector encoding c-src was used to transduce *c-jun*$^{-/-}$ cells, and cellular motility was assessed. Transduction of *c-jun*$^{-/-}$ with a c-Src expression vector increased c-Src abundance to a level similar to that of *c-jun*$^{f/f}$ cells (Figure 10A). Associated with the transduction of

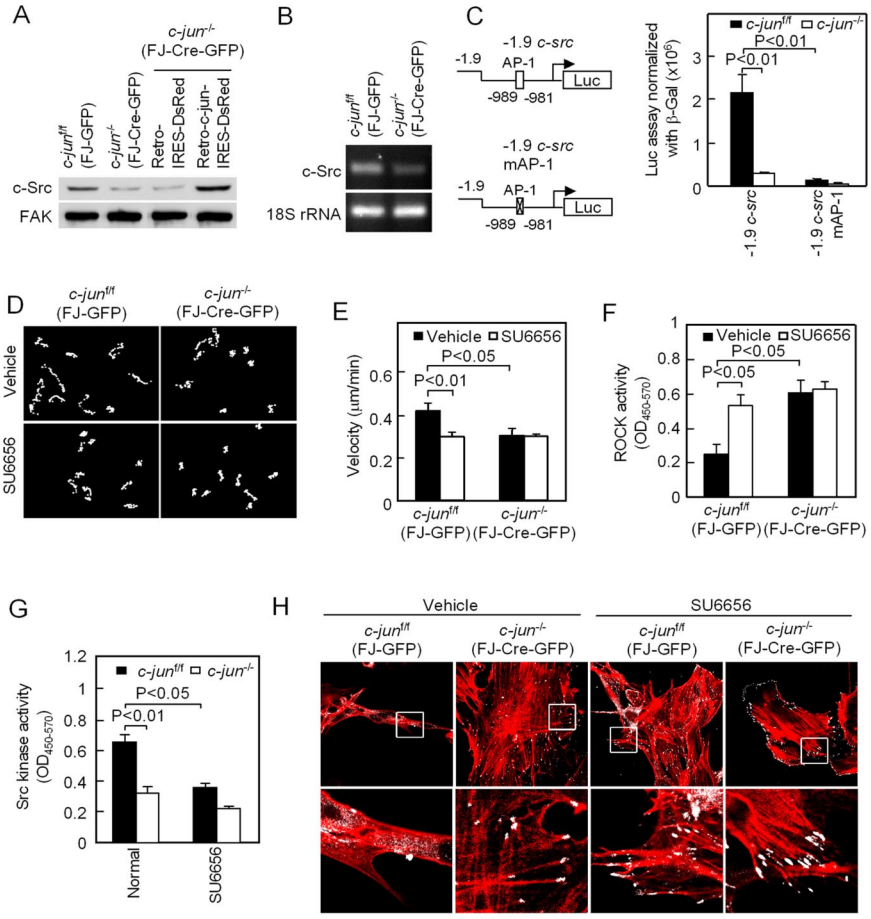


**Figure 9.** c-jun induces Src expression and signaling. (A) Western blot analysis of *c-jun*$^{f/f}$ or *c-jun*$^{-/-}$ cells for abundance of c-Src with FAK or guanine dissociation inhibitor (GDI; not shown) used as a loading control for protein abundance. *c-jun*$^{-/-}$ cells were transduced with either a control vector (Retro-IRES-GFP) or c-Jun expression vector (Retro-c-Jun-IRES-DsRed) and examined for c-Src abundance by Western blot. (B) c-Src mRNA abundance determined by RT-PCR. (C) Schematic representation of the human *c-src* promoter or AP-1 site point mutant *c-src* promoter luciferase reporter. Relative luciferase activity was determined by transient transfection of *c-jun*$^{-/-}$ or *c-jun*$^{+/+}$ cells. Cellular migration (D), migratory velocity (E), ROCK activity (F), Src kinase activity (G). (H) Costaining with F-actin (rhodamine phalloidin in red) and paxillin (in white). Treatment of *c-jun*$^{+/+}$ cells with c-Src kinase inhibitor reduces cellular migration and velocity (D and E), Src kinase activity (G), induces ROCK activity (F), and induces formation of stable focal contacts characterized by paxillin staining at the end of large F-actin cables (H).

*c-jun*$^{-/-}$ cells with the c-Src expression vector, the cellular morphology by phase-contrast microscopy demonstrated the restoration of the polarized morphology of *c-jun*$^{f/f}$ cells (Figure 10B). Single-cell videomicroscopy was conducted on *c-jun*$^{-/-}$ cells transduced with either control or c-Src expression vector (Figure 10C). *c-jun*$^{-/-}$ cellular velocity was enhanced two-fold upon transduction with a retrovirus encoding c-Src (Figure 10C). c-Src expression increased Src kinase activity, reduced the enhanced F-actin staining of *c-jun*$^{-/-}$ cells, and reduced ROCK kinase activity (Figure 10, D and E).

To determine whether endogenous c-jun regulated the morphology and cellular migratory velocity of epithelial cells, primary MEC cultures were made from *c-jun*$^{f/f}$ mice. Cells were transduced with adenoviral expression vectors encoding either Cre or control empty virus. PCR analysis identified the presence of the ~600-bp *c-jun* fragment created through excision of the floxed c-jun allele (Figure 11A). Western blot analysis demonstrated a dramatic reduction in c-Jun abundance and a ~50% reduction in c-Src abundance (Figure 11B). Wounding assays were conducted, and single-cell migration analysis was conducted by videomicroscopy (Figure 11, C and D). The cellular velocity of MEC was reduced ~25% upon deletion of *c-jun*. The magnitude of the difference in velocity gradually decreased as cells filled the wound with maximal difference at the initial time point analyzed 4 h after wounding (Figure 11E). Thus endogenous c-jun promotes cellular migratory velocity in both fibroblasts and epithelial cells.

Collectively these studies suggest endogenous c-Jun induces c-Src abundance, thereby inhibiting ROCK activity, reducing phosphorylation of cofilin and stress fiber formation to promote a more motile phenotype (Figure 12).

## DISCUSSION

The *c-jun* protooncogene encodes the founding member of the AP-1 family (Angel and Karin, 1991). c-Jun overexpression is common in human tumors and promotes cellular proliferation and DNA synthesis (Angel and Karin, 1991). Disruption of the *c-jun* gene in murine hepatocytes prevents the emergence of hepatocellular carcinoma (Eferl *et al.*, 2003), and c-Jun is sufficient for the induction of anchorage-independent growth of Rat1a cells (Kinoshita *et al.*, 2003). The mechanisms by which c-Jun contributes to tumor progression through regulation of cellular apoptosis is known to involve p53 and p21$^{CIP1}$ (Eferl *et al.*, 2003). c-Jun is known to promote cellular migration; however, the role of endogenous c-Jun in cellular invasion and the intracellular signaling pathway involved was previously unknown. The current studies demonstrate c-Jun promotes cellular invasion and migration through the induction of c-Src and at least in part the inhibition of ROCK II kinase (Figure 10). Endogenous c-Jun functions to attenuate hyperactive ROCK-mediated induction of large, stable centripetally distributed focal contacts, to enhance focal contact turnover and promote cellular migration and invasion (Figure 10).

The current studies demonstrate c-Jun induces c-Src abundance, raising the possibility that the induction of AP-1 activity and c-Jun expression in tumors may contribute to increased cellular invasiveness. Consistent with this model, reintroduction of c-Src into *c-jun*$^{-/-}$ cells by retroviral trans-

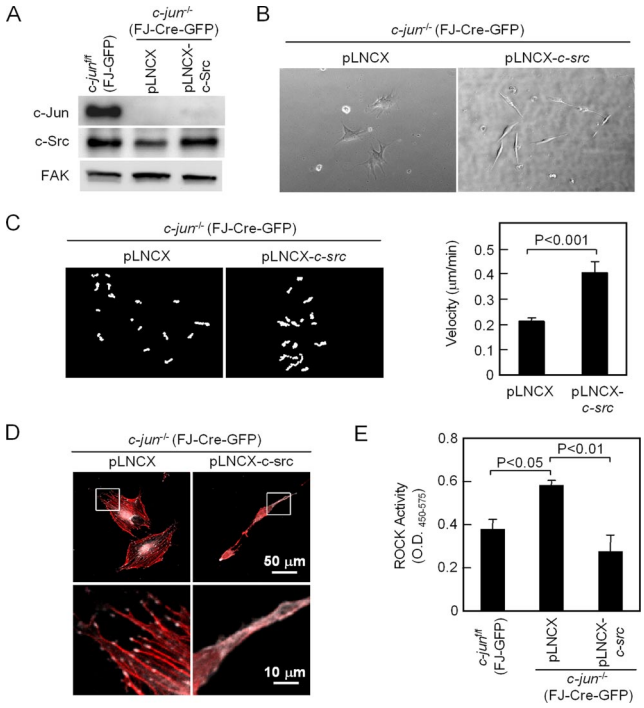


**Figure 10.** c-Src rescues the morphological abnormality and migration defect of *c-jun*$^{-/-}$ cells. (A) Western blot of *c-jun*$^{-/-}$ cells transduced with control vector or c-Src retroviral expression vector. (B) Phase-contrast and (C) single-cell video analysis (left) and migration velocity (right) of *c-jun*$^{-/-}$ cells transduced with pLNCX-c-Src. (D) F-actin staining and Src-kinase assays demonstrating induction of c-Src kinase activity by c-Jun. (E) Restoration of c-Src reduced ROCK kinase activity of *c-jun*$^{-/-}$ cells.

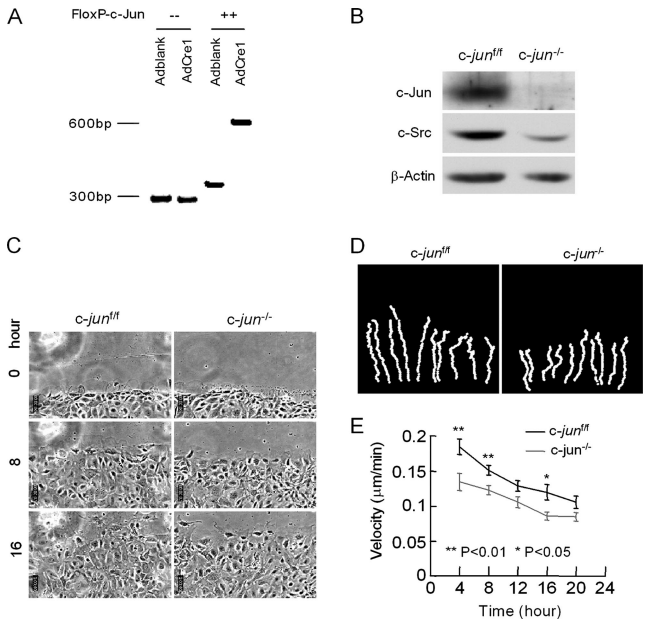


**Figure 11.** c-Jun deletion reduces migration of primary murine mammary epithelial cells. Primary murine mammary epithelial cells of *c-Jun*$^{f/f}$ mice transduced with adenoviral-IRES-GFP vectors expressing either GFP or Cre and GFP were examined by genomic analysis for the presence of a 600-base pair band indicative of *c-jun* excision using PCR (A) and Western blot (B). (C and D) Cellular migration into a wound. (E) Single-cell migratory behavior quantification for cellular velocity. Deletion of endogenous c-jun reduced cellular velocity from 0.185 ± 0.011 to 0.135 ± 0.012 $\mu$m/min in the first 4 h ($p < 0.01$).

duction, reverted the spread morphology to the polar fibroblastoid morphology, associated with the induction of c-Src abundance by Western blot (data not shown). The cellular homologue of the transforming v-Src, c-Src, is widely expressed in mammalian cells, is rarely mutated, but is commonly increased in abundance or catalytic activity in human cancer (Ishizawar and Parsons, 2004). The Src family tyrosine kinases (SFK) have been implicated in cellular adhesion during animal development. SRC-1, the *Caenorhabditis elegans* SFK orthologue, is required for cell migration (Itoh *et al.*, 2005). c-Src phosphorylation promotes cell migration through phosphorylating distinct substrates including Endophilin A2, Crk-associated substrate (Cas), ZRP-1 (Zyxin-related protein1) and altering the spatial regulation of $\beta$-actin translation through ZBP1. The mechanism responsible for the induction of c-Src abundance in human cancer is not well understood, but elevated abundance has been found in human cancers including lung, skin, colon, breast, endometrial, and head and neck malignancies.

c-Jun induced c-Src (Figure 9A) and repressed ROCK II expression and activity, evidenced by a reduction in phosphorylation of cofilin and the myosin-binding subunit of myosin phosphatase. ROCK activates LIMK which phosphorylates cofilin, inhibiting its actin-depolymerizing activity, thereby stabilizing actin stress fibers. Consistent with our findings, v-Src inhibited cofilin phosphorylation and the mechanism involved a MEK-dependent and PI3 kinase-independent pathway (Pawlak and Helfman, 2002). Rho mutants restore stress fiber formation in v-Src–transformed cells (Mayer *et al.*, 1999), consistent with a model in which Rho proteins serve as downstream targets of v-Src. In our studies, c-Jun reintroduction into *c-jun*$^{-/-}$ cells inhibited Rho kinase activity and induced cellular migration. Silenc-

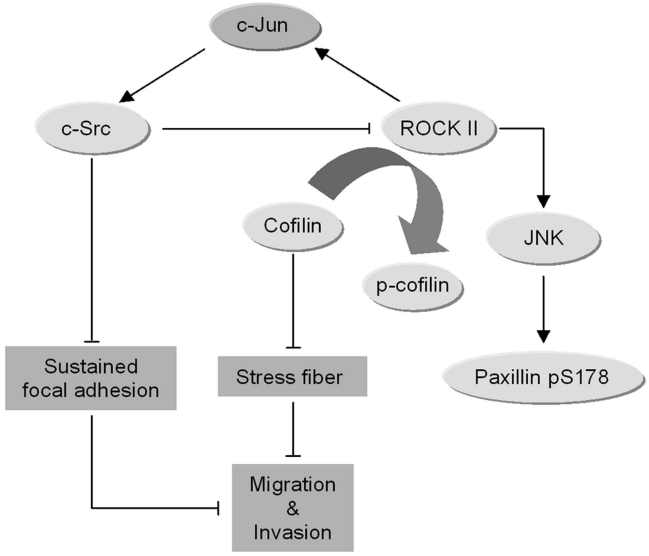


**Figure 12.** Proposed model by which endogenous c-Jun regulates cellular migration. c-Jun induces c-Src expression and activity. c-Src activity inhibits ROCK activity, consequently reducing phosphorylation of cofilin, reducing hyperactive stress fiber formation, and promoting cellular migration and invasion. ROCK induces c-Jun expression (Marinissen *et al.*, 2004). Endogenous c-Jun–mediated inhibition of c-Src expression would be predicted to function in a homeostatic feedback to normalize c-Jun induction by ROCK.

ing of the c-jun heterodimeric partner Fra1 also reduces cell motility and hyperactivates Rho-ROCK, leading to increased stress fiber formation and stabilization of focal adhesion (Vial *et al.*, 2003). Fra1 promoted cell motility by inhibiting RhoA. The reduction in RhoA activity in Ras-transformed cells is necessary for the increased motility of Ras-transformed cells (Sahai *et al.*, 2001). In Ras-transformed cells the reduction in Rho kinase activity is associated with a translocation of ROCK and Rho kinase from the triton-soluble to the Triton X-100–insoluble fraction through an unknown mechanism, further contributing to the reduction in ROCK activity (Sahai *et al.*, 2001). Although speculative, caveolae are located in the X-100 membrane-insoluble fraction and c-Src within caveolae is thought to be inactive. It will be of interest to determine whether the peripherally located phosphorylated paxillin colocalizes with caveolae.

The inhibition of RhoA by c-Src is known to contribute to remodeling of focal contacts. The increased migratory velocity of c-Jun–expressing cells is consistent with the finding that ROCK kinase inhibitors enhance migratory velocity (Totsukawa *et al.*, 2004). The enhancement of migratory velocity of ROCK kinase inhibited cells correlated with a reduction in stable mature focal adhesions, which probably function as a "brake" on the cell migration machinery. Integrin aggregation, for example, via tissue transglutaminase (tTG) inhibits Src kinase-elevating RhoA (Janiak *et al.*, 2006). Cells treated with tTG, like *c-jun*$^{-/-}$ cells, display elevated RhoA/ROCK II, activity, reduced c-Src activity, and prominent stress fibers, with increased focal adhesions (Janiak *et al.*, 2006). Thus, c-Jun by regulating c-Src, may in turn modulate the cooperative interaction between integrins and surface tTG.

The inhibition of ROCK activity by endogenous c-Jun may function as an important homeostatic feedback mechanism. ROCK activates JNK, which phosphorylates c-Jun and ATF2, to induce c-Jun expression (Marinissen *et al.*, 2004). RhoA stimulation of ROCK occurs independently of the ability of ROCK to promote actin polymerization. Similarly, ROCK activation leads to phosphorylation of the actin-depolymerizing factor cofilin and the stabilization of polymerized F-actin (Sotiropoulos *et al.*, 1999). The consequent reduction in the monomeric G-actin pool is sensed by SRF, which induces c-Fos expression (Miralles *et al.*, 2003). Thus ROCK would be predicted to induce AP-1 activity in a sustained feed-forward manner. Through the induction of c-Src, and consequent inhibition of ROCK by endogenous c-Jun as shown herein, a homeostatic mechanism exists to attenuate, in a physiological manner, AP-1 activation induced by diverse stimuli.

## ACKNOWLEDGMENTS

We thank Dr. M. Karin for plasmids and helpful advice and Almeta Mathis for assistance in preparing the manuscript. The work was supported in part by Grants R01CA70896, R01CA75503, R01CA86072 (R.G.P.). The Kimmel Cancer Center was supported by the National Institutes of Health (NIH) Cancer Center Core Grant P30CA56036 (R.G.P.) and previously the Lombardi Comprehensive Cancer Center was supported by the NIH Comprehensive Cancer Center Core Grant CA51008-13 (R.G.P.). This project is funded in part from the Dr. Ralph and Marian C. Falk Medical Research Trust and a grant from Pennsylvania Department of Health (R.G.P.). The Department specifically disclaims responsibility for any analysis, interpretations, or conclusions.

## REFERENCES

Albanese, C. *et al.* (1999). Activation of the *cyclin D1* gene by the E1A-associated protein p300 through AP-1 inhibits cellular apoptosis. J. Biol. Chem. *274*, 34186–34195.

Alper, O., and Bowden, E. T. (2005). Novel insights into c-Src. Curr. Pharmaceut. Design *11*, 1119–1130.

Amano, M., Chihara, K., Kimura, K., Fukata, Y., Nakamura, N., Matsuura, Y., and Kaibuchi, K. (1997). Formation of actin stress fibers and focal adhesions enhanced by Rho-kinase. Science *275*, 1308–1311.

Angel, P., and Karin, M. (1991). The role of Jun, Fos and the AP-1 complex in cell-proliferation and transformation. Biochim. Biophys. Acta *1072*, 129–157.

Balkwill, F. (2004). Cancer and the chemokine network. Nat. Rev. Cancer *4*, 540–550.

Beningo, K. A., Dembo, M., Kaverina, I., Small, J. V., and Wang, Y. L. (2001). Nascent focal adhesions are responsible for the generation of strong propulsive forces in migrating fibroblasts. J. Cell Biol. *153*, 881–888.

Bowden, E. T., Coopman, P. J., and Mueller, S. C. (2001). Invadopodia: unique methods for measurement of extracellular matrix degradation in vitro. Methods Cell Biol. *63*, 613–627.

Brown, J. R., Nigh, E., Lee, R. J., Ye, H., Thompson, M. A., Saudou, F., Pestell, R. G., and Greenberg, M. E. (1998). Fos family members induce cell cycle entry by activating cyclin D1. Mol. Cell. Biol. *18*, 5609–5619.

Brown, M. C., and Turner, C. E. (2004). Paxillin: adapting to change. Physiol. Rev. *84*, 1315–1339.

Eferl, R., Ricci, R., Kenner, L., Zenz, R., David, J. P., Rath, M., and Wagner, E. F. (2003). Liver tumor development. c-Jun antagonizes the proapoptotic activity of p53. Cell *112*, 181–192.

Eferl, R., and Wagner, E. F. (2003). AP-1, a double-edged sword in tumorigenesis. Nat. Rev. Cancer *3*, 859–868.

Egeblad, M., and Werb, Z. (2002). New functions for the matrix metalloproteinases in cancer progression. Nat. Rev. Cancer *2*, 161–174.

Fu, M., Wang, C., Li, Z., Sakamaki, T., and Pestell, R. G. (2004). Minireview: Cyclin D1, normal and abnormal functions. Endocrinology *145*, 5439–5447.

Ishizawar, R., and Parsons, S. J. (2004). c-Src and cooperating partners in human cancer. Cancer Cell *6*, 209–214.

Itoh, B., Hirose, T., Takata, N., Nishiwaki, K., Koga, M., Ohshima, Y., and Okada, M. (2005). SRC-1, a non-receptor type of protein tyrosine kinase, controls the direction of cell and growth cone migration in *C. elegans.* Development *132*, 5161–5172.

Janiak, A., Zemskov, E. A., and Belkin, A. M. (2006). Cell surface transglutaminase promotes RhoA activation via integrin clustering and suppression of the Src-p190RhoGAP signaling pathway. Mol. Biol. Cell *17*, 1606–1619.

Ju, X. *et al.* (2007). Akt1 governs breast cancer progression in vivo. Proc. Natl. Acad. Sci. USA *104*, 7438–7443.

Karin, M., Liu, Z., and Zandi, E. (1997). AP-1 function and regulation. Curr. Opin. Cell Biol. *9*, 240–246.

Katiyar, S., Jiao, X., Wagner, E., Lisanti, M. P., and Pestell, R. G. (2007). Somatic excision demonstrates c-Jun induces cellular migration and invasion through induction of stem cell factor. Mol. Cell. Biol. *27*, 1356–1369.

Kinoshita, I., Leaner, V., Katabami, M., Manzano, R. G., Dent, P., Sabichi, A., and Birrer, M. J. (2003). Identification of cJun-responsive genes in Rat-1a cells using multiple techniques: increased expression of stathmin is necessary for cJun-mediated anchorage-independent growth. Oncogene *22*, 2710–2722.

Kolbus, A., Herr, I., Schreiber, M., Debatin, K. M., Wagner, E. F., and Angel, P. (2000). c-Jun-dependent CD95-L expression is a rate-limiting step in the induction of apoptosis by alkylating agents. Mol. Cell. Biol. *20*, 575–582.

Kumagai, N., Ohno, K., Tameshige, R., Hoshijima, M., Yogo, K., Ishida, N., and Takeya, T. (2004). Induction of mouse c-src in RAW264 cells is dependent on AP-1 and NF-kappaB and important for progression to multinucleated cell formation. Biochem. Biophys. Res. Commun. *325*, 758–768.

Lakkakorpi, P. T., Nakamura, I., Young, M., Lipfert, L., Rodan, G. A., and Duong, L. T. (2001). Abnormal localisation and hyperclustering of (alpha)(V)(beta)(3) integrins and associated proteins in Src-deficient or tyrphostin A9-treated osteoclasts. J. Cell Sci. *114*, 149–160.

Li, Z., Jiao, X., Wang, C., Ju, X., Lu, Y., Lisanti, M., Katiyar, S., and Pestell, R. G. (2006a). Cyclin D1 induction of cellular migration requires p27$^{KIP1}$. Cancer Res. *66*, 9986–9994.

Li, Z. *et al.* (2006b). Cyclin D1 regulates cellular migration through the inhibition of thrombospondin 1 and ROCK signaling. Mol. Cell. Biol. *26*, 4240–4256.

Lin, E. H., Hui, A. Y., Meens, J. A., Tremblay, E. A., Schaefer, E., and Elliott, B. E. (2004). Disruption of $Ca^{2+}$-dependent cell-matrix adhesion enhances c-Src kinase activity, but causes dissociation of the c-Src/FAK complex and dephosphorylation of tyrosine-577 of FAK in carcinoma cells. Exp. Cell Res. *293*, 1–13.

Maeda, S., and Karin, M. (2003). Oncogene at last—c-Jun promotes liver cancer in mice. Cancer Cell *3*, 102–104.

Mammoto, A., Huang, S., Moore, K., Oh, P., and Ingber, D. E. (2004). Role of RhoA, mDia, and ROCK in cell shape-dependent control of the Skp2-p27kip1 pathway and the G1/S transition. J. Biol. Chem. *279*, 26323–26330.

Marinissen, M. J., Chiariello, M., Tanos, T., Bernard, O., Narumiya, S., and Gutkind, J. S. (2004). The small GTP-binding protein RhoA regulates c-jun by a ROCK-JNK signaling axis. Mol. Cell *14*, 29–41.

Mayer, T., Meyer, M., Janning, A., Schiedel, A. C., and Barnekow, A. (1999). A mutant form of the rho protein can restore stress fibers and adhesion plaques in v-src transformed fibroblasts. Oncogene *18*, 2117–2128.

Miralles, F., Posern, G., Zaromytidou, A. I., and Treisman, R. (2003). Actin dynamics control SRF activity by regulation of its coactivator MAL. Cell *113*, 329–342.

Neumeister, P. *et al.* (2003). Cyclin D1 governs adhesion and motility of macrophages. Mol. Biol. Cell *14*, 2005–2015.

Pawlak, G., and Helfman, D. M. (2002). MEK mediates v-Src-induced disruption of the actin cytoskeleton via inactivation of the Rho-ROCK-LIM kinase pathway. J. Biol. Chem. *277*, 26927–26933.

Pestell, R. G., Albanese, C., Reutens, A. T., Segall, J. E., Lee, R. J., and Arnold, A. (1999). The cyclins and cyclin-dependent kinase inhibitors in hormonal regulation of proliferation and differentiation. Endocr. Rev. *20*, 501–534.

Playford, M. P., and Schaller, M. D. (2004). The interplay between Src and integrins in normal and tumor biology. Oncogene *23*, 7928–7946.

Qi, J., Wang, J., Romanyuk, O., and Siu, C. H. (2006). Involvement of Src family kinases in N-cadherin phosphorylation and beta-catenin dissociation during transendothelial migration of melanoma cells. Mol. Biol. Cell *17*, 1261–1272.

Ren, X. D., Kiosses, W. B., Sieg, D. J., Otey, C. A., Schlaepfer, D. D., and Schwartz, M. A. (2000). Focal adhesion kinase suppresses Rho activity to promote focal adhesion turnover. J. Cell Sci. *113*(Pt 20), 3673–3678.

Riabowol, K. T., Vosatka, R. J., Ziff, E. B., Lamb, N. J., and Feramisco, J. R. (1988). Microinjection of *fos*-specific antibodies blocks DNA synthesis in fibroblast cells. Mol. Cell. Biol. *8*, 1670–1676.

Ridley, A. J., and Hall, A. (1992). The small GTP-binding protein rho regulates the assembly of focal adhesions and actin stress fibers in response to growth factors. Cell *70*, 389–399.

Sahai, E., and Marshall, C. J. (2002). ROCK and Dia have opposing effects on adherens junctions downstream of Rho. Nat. Cell Biol. *4*, 408–415.

Sahai, E., Olson, M. F., and Marshall, C. J. (2001). Cross-talk between Ras and Rho signalling pathways in transformation favours proliferation and increased motility. EMBO J. *20*, 755–766.

Schlaepfer, D. D., Mitra, S. K., and Ilic, D. (2004). Control of motile and invasive cell phenotypes by focal adhesion kinase. Biochim. Biophys. Acta *1692*, 77–102.

Sluss, H. K., and Davis, R. J. (1997). Embryonic morphogenesis signaling pathway mediated by JNK targets the transcription factor JUN and the TGF-beta homologue decapentaplegic. J. Cell Biochem. *67*, 1–12.

Smilenov, L. B., Mikhailov, A., Pelham, R. J., Marcantonio, E. E., and Gundersen, G. G. (1999). Focal adhesion motility revealed in stationary fibroblasts. Science *286*, 1172–1174.

Sotiropoulos, A., Gineitis, D., Copeland, J., and Treisman, R. (1999). Signal-regulated activation of serum response factor is mediated by changes in actin dynamics. Cell *98*, 159–169.

Totsukawa, G., Wu, Y., Sasaki, Y., Hartshorne, D. J., Yamakita, Y., Yamashiro, S., and Matsumura, F. (2004). Distinct roles of MLCK and ROCK in the regulation of membrane protrusions and focal adhesion dynamics during cell migration of fibroblasts. J. Cell Biol. *164*, 427–439.

Vial, E., Sahai, E., and Marshall, C. J. (2003). ERK-MAPK signaling coordinately regulates activity of Rac1 and RhoA for tumor cell motility. Cancer Cell *4*, 67–79.

Wulf, G., Garg, P., Liou, Y.-C., Iglehart, D., and Lu, K. P. (2004). Modeling breast cancer in vivo and ex vivo reveals an essential role of Pin1 in tumorigenesis. EMBO J. *23*, 3397–3407.

Xia, Y., and Karin, M. (2004). The control of cell motility and epithelial morphogenesis by Jun kinases. Trends Cell Biol. *14*, 94–101.